42nd AIAA Fluid Dynamics Conference and Exhibit
25 - 28 June 2012, New Orleans, Louisiana

AIAA 2012-3148

A Preliminary Study of the Longitudinal Merging of Instability Wave Packets and Turbulent Spots in a Hypersonic Boundary Layer

Katya M. Casper*
School of Aeronautics and Astronautics, Purdue University, West Lafayette, IN 47907-1282
Sandia National Laboratories, Albuquerque, NM 87185

Steven J. Beresh†
Sandia National Laboratories, Albuquerque, NM 87185

Steven P. Schneider‡
School of Aeronautics and Astronautics, Purdue University, West Lafayette, IN 47907-1282

The longitudinal merging of wave packets and turbulent spots in a hypersonic boundary layer was studied on the nozzle wall of the Boeing/AFOSR Mach-6 Quiet Tunnel. Two pulsed glow perturbations were created in rapid succession to generate two closely spaced disturbances. The time between the perturbations was varied from run to run to simulate longitudinal merging. Preliminary results suggest that the growth of the trailing disturbance seems to be suppressed by the presence of the leading disturbance. Conversely, the core of the leading disturbance appears unaffected by the presence of the trailing disturbance and behaves as if isolated. This result is consistent with low-speed studies as well as DNS computations of longitudinal merging. However, the present results may be influenced by the perturber performance and therefore further studies of longitudinal merging are necessary to confirm the effect on the internal pressure structure of the interacting disturbances.

Nomenclature

M	freestream Mach number	y	tunnel spanwise coordinate measured from the centerline of the perturber along the circumference of the wall, positive to the right looking upstream (m)
p'	pressure fluctuation, $p - p_\infty$ (Pa)		
p_∞	freestream static pressure (Pa)		
P_0	tunnel stagnation pressure (kPa)		
Re	freestream unit Reynolds number (1/m)	$\tilde{z}$	tunnel axial coordinate with variable origin (m)
T_0	tunnel stagnation temperature (K)	z	tunnel axial coordinate measured from throat (m)
Δt_p	time between pairs of glow perturbations (ms)		
U_∞	freestream velocity (m/s)		

*Research Assistant and Sandia Graduate Intern, Student Member AIAA, kcasper@purdue.edu, (765) 494-3348
†Principal Member of the Technical Staff, Engineering Sciences Center, Associate Fellow AIAA
‡Professor, Associate Fellow AIAA

Sandia National Laboratories is a multi-program laboratory managed and operated by Sandia Corporation, a wholly owned subsidiary of Lockheed Martin Corporation, for the U.S. Department of Energy's National Nuclear Security Administration under contract DE-AC04-94AL85000.

I. Introduction

Hypersonic reentry vehicles are subjected to high levels of fluctuating pressures. These intense fluctuations can cause vibration of internal components and lead to structural problems. There is a need to predict the magnitude, location, and spatial extent of the pressure fluctuations to better design hypersonic flight vehicles. Current designs often use overly conservative estimates of the fluctuations which lead to heavier vehicles and degraded flight performance. Some correlations exist for the magnitude of transitional and turbulent pressure fluctuations, but these were derived primarily using either incompressible data or conventional (noisy flow) hypersonic wind-tunnel tests.[1] Such modeling efforts have not led to sufficient physical understanding of the transitional pressure fluctuations or to adequate predictive capabilities.

Wind-tunnel tests at fixed freestream conditions have shown that transitional pressure fluctuations can be more severe than turbulent pressure fluctuations,[2–6] making transitional fluctuations of primary interest for this work. The transition process can be described through intermittency and the growth and propagation of turbulent spots in the transitional boundary layer.[7] These turbulent spots create wall pressure fluctuations. By combining the pressure fluctuations associated with wave packets and turbulent spots into a model of transition, the models can be extended to calculate transitional pressure fluctuations from fundamental physics. This type of model has already been developed for incompressible flow on a flat plate.[8]

Recent direct numerical simulation (DNS) efforts have computed the pressure field for wave packets and developing turbulent spots in hypersonic boundary layers.[9–12] Recent experimental measurements have also measured the internal structure of spots in pressure data under a hypersonic boundary layer.[13–16] These measurements were made on the nozzle wall of the Boeing/AFOSR Mach-6 Quiet Tunnel (BAM6QT). Under quiet flow operation, laminar boundary layers are maintained on the wall of the wind tunnel. A pulsed glow perturber was used to create controlled perturbations on the nozzle wall. The resulting instability wave packets were measured along with their development into turbulent spots, including centerline and spanwise measurements.

This study extends that work by looking at the longitudinal merging of two disturbances. The interaction and merging of two turbulent spots is an important parameter for a spot model of transition. Classical intermittency models of transition assume that turbulent spots are independent. When they merge, the region covered by turbulence is the superposition of the two turbulent spots.[7,17,18] Also, the internal structure of the spot is typically assumed to remain constant.[8] However, low-speed experiments and recent DNS simulations have shown that this may not be the case.[19–23] Turbulent spots actually influence the development and growth of adjacent spots. In addition, there is a difference between lateral and longitudinal merging of spots. In the lateral merging case, the interacting wingtips of the spot have larger upwash than an isolated spot. This creates an inflectional velocity profile that generates new spanwise structures to tie the lateral spots together.[22] This would affect the internal structure of the spots as they merge. In the longitudinal merging case, the growth of the upstream spot was found to be suppressed in the calmed region of the downstream spot.[23] This suppression affects both the spot footprint as well as the magnitude of fluctuations within the spots. Measurements are needed to determine how the pressure-fluctuation field and the spatial footprint of the disturbances is affected by this merging in a hypersonic boundary layer and how this compares to simple superposition of the disturbances.

In order to study longitudinal merging, disturbances can be generated in quick succession by a rapid repetition of a glow perturbation. Because the disturbances develop from wave packets into spots further downstream, these measurements show the growth of a trailing disturbance in the wake of a leading disturbance. Such disturbances may be either instability waves or turbulent spots. The second disturbance can be generated at different time intervals behind the first disturbance to simulate longitudinal merging. Unfortunately, the current experimental setup does not allow a study of lateral spot merging, which would require construction of additional tunnel hardware to place a second perturber on the nozzle wall. Also, in order to have a large region of lateral interaction, a longer measurement region is needed for disturbances to grow in the lateral direction. However, by studying longitudinal merging, a better understanding of the transitional physics can be gained that can then be included in engineering models for predicting a flight vehicle's environment.

II. Experimental Setup

A. Boeing/AFOSR Mach-6 Quiet Tunnel

Measurements were made on the nozzle wall of the Boeing/AFOSR Mach-6 Quiet Tunnel (Fig. 1). This tunnel is one of two hypersonic quiet tunnels in the world. Because it can be operated as a conventional noisy tunnel or as a quiet tunnel, freestream noise effects can be studied. The tunnel is a Ludwieg tube – a long pressurized tube with a converging-diverging nozzle on the end. The flow passes from the driver tube, through the test section, diffuser, and finally to the vacuum tank. Flow is initiated by bursting a double diaphragm that is located downstream of the diffuser. When the flow begins, an expansion wave travels upstream and then reflects between the upstream end of the driver tube and the contraction. The total pressure and temperature drop with each reflection cycle (every 200 ms) until the tunnel unstarts. Run times of 3–5 s are typical under quiet-flow conditions at present. The tunnel uses air as the test gas and operates with an initial total pressure P_0 of 34–2070 kPa and an initial total temperature T_0 of 430 K. These conditions give a freestream unit Reynolds number range of $0.4–18.3 \times 10^6$/m, calculated using Keyes's law for viscosity.[24] The current maximum quiet stagnation pressure is 1170 kPa. The test-section diameter is 0.242 m at the nozzle exit, and the nozzle is 2.590 m long. Noise levels vary from 2–4.5% under noisy-flow conditions. Under quiet-flow conditions, noise levels are 0.05% or less.[25]

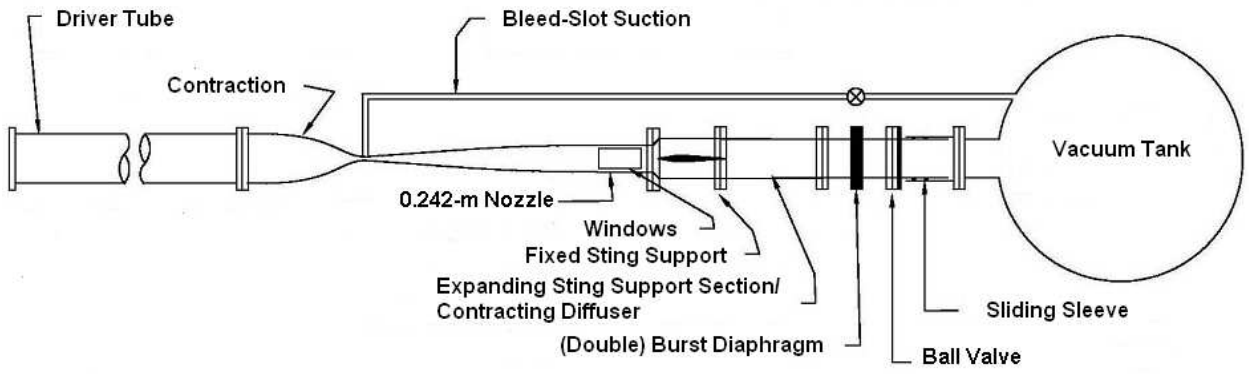

Figure 1. Boeing/AFOSR Mach-6 Quiet Tunnel.

Obtaining quiet flow in a hypersonic tunnel is not a trivial task. The nozzle is polished to a mirror finish to avoid roughness-induced transition, and the contraction boundary layer is removed by bleed slots at the throat. A new laminar boundary layer then begins just upstream of the nozzle throat and is maintained through the test section. In addition, the air is filtered to remove dust or other particles above 0.01 microns that may damage the nozzle or trip the boundary layer. More details about the development of the BAM6QT can be found in Schneider.[26]

B. Controlled Generation of Wave Packets and Turbulent Spots using a Pulsed Glow Perturber

In order to create flow perturbations that lead to formation of instability wave packets and turbulent spots within the length of the test section, a pulsed glow perturber is used. The perturber uses an electrode design that isolates the ground from the tunnel, reducing electrical noise during the perturbation. This design has two 1.1-mm diameter stainless steel electrodes in a Macor mount. The spacing between electrodes is 1.3 mm. The perturber uses an ignition coil and timing circuit to create perturbations. The ignition coil always remains charged until a perturbation is desired. When the coil is suddenly shut off, a high voltage output is created. This voltage is passed through a resistive suppressor spark plug to limit the current output before passing to the electrodes.

The glow perturbation is typically created at 200 Hz to allow measurements of the resulting disturbances in the intervals between the electro-magnetic interference generated by the perturbation. The perturbation is turned off while disturbances convect downstream over the sensors. In order to simulate longitudinal

merging, pairs of perturbations were created with Δt_p = 1.0, 0.5, 0.33 and 0.25 ms between them. This pattern was repeated at 200 Hz, consistent with the isolated disturbances studied previously.[13–16]

In order to better characterize the perturbation being input into the flow, voltage and current measurements were made. The current across the electrodes was measured using a Bergoz CT-D1.0 current transformer. This current transformer has a sensitivity of 1V/A and can resolve frequencies between 200 Hz and 500 MHz. The transformer can measure a maximum current of 1000 A and a maximum RMS current of 11 A. The voltage across the electrodes was measured using a Tektronix P6015 High-Voltage Probe. This probe is a 1000× attenuator probe that can resolve frequencies between 0 and 75 MHz. Voltages up to 20 kV DC or 40 kV RMS can be measured. The voltage was measured between the electrode wires running from the perturber. Together, these measurements give the current and voltage of the perturbation as a function of time, allowing the computation of the perturbation power and energy.

C. Instrumentation and Data Acquisition

Kulite XCQ-062-15A pressure transducers are used to measure surface pressure fluctuations. These transducers use silicon diaphragms as the basic sensing mechanisms. Each diaphragm contains a fully active four-arm Wheatstone bridge. The sensors are mechanically stopped above 103 kPa to prevent damage to the diaphragms at the high BAM6QT pre-run pressures. They have a resonant frequency between 250–300 kHz. The repeatability of the sensors is approximately 0.1% of the full scale, or 0.1 kPa. The Kulites have screens to protect the diaphragms from damage. For these tests, only A-screen sensors were used. The A-screen has a large central hole. This screen offers only a small amount of diaphragm protection, but the sensor has a flatter frequency response up to 30–40% of the resonant frequency.[27] The sensitive area of the A-screen sensor is the hole size (0.81 mm^2). The Kulites are only used to obtain the AC signal. The sensors have a repeatable, linear calibration slope which can be used to determine the fluctuating component of the signal (within the flat dynamic range of the sensor).[28] The fluctuations were normalized by the freestream pressure, computed using the total pressure and freestream Mach number in the tunnel.

The signal from the Kulite pressure transducers was processed by custom-built electronics, which also supply a 10 V excitation. The output signal was amplified by a gain of 100 with an INA103 instrumentation amplifier chip to give the DC signal. Tektronix TDS7104, DPO7104, two TDS5034B, and two DPO7054 Digital Phosphor Oscilloscopes were used for data acquisition. The scopes have an 8-bit vertical resolution, but the resolution can be increased to over 11 bits in Hi-Res mode. Hi-Res mode is also used to provide digital filtering. The oscilloscopes average in real time at the maximum sampling rate of 1.25–5 GS/s (depending on the model) for 4 input channels and then save data at the specified sampling rate. The data sampling rate for these measurements was 500 kHz. Pressure traces were post-processed by low-pass filtering the data at 150 kHz using an 8-pole digital Butterworth filter (48 dB of attenuation per octave). This filtering removes sensor diaphragm resonance from the pressure traces to show the underlying data more clearly.

D. Nozzle Wall Setup

A schematic of the experimental setup is shown in Fig. 2. The perturber is placed on the top wall of the tunnel at z = 1.924 m, where z is the axial tunnel coordinate measured from the throat. There is a small spanwise insert at z = 2.055 m, downstream of the perturber electrodes (Fig. 3(a)). This spanwise insert has locations for sensors at y = ± 2.5, 5.1, 7.6, 10.1, 15.2, and 20.2 mm, where y is measured from the centerline of the perturber position along the circumference of the wall. Downstream, there are various sensor locations along the tunnel centerline in a slender traverse plug insert. There is also a cylindrical pipe insert that was designed to fit between the nozzle exit and the diffuser sting support to extend the testing length as shown in Figs. 2 and 3(b). This insert has the same diameter of 0.242 m as the nozzle exit. When the tunnel is closed, the pipe insert fits flush with the nozzle exit and extends 0.254 m downstream. This pipe insert is actually made of five rings. One of the downstream rings has azimuthal sensor locations at y = ± 11, 21, 32, 42, and 63 mm. The four downstream rings are interchangeable to allow azimuthal measurements at any of the four downstream locations. For spanwise measurements of longitudinal merging, this spanwise array was located at z = 2.781 m. Centerline measurements were made at z = 2.055, 2.730, 2.781 and 2.831 m.

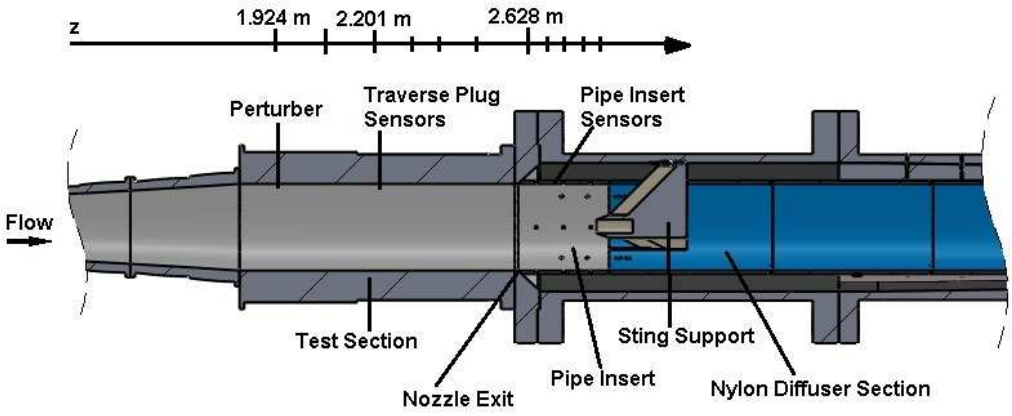

Figure 2. Schematic of experimental setup in the BAM6QT for nozzle-wall measurements. Perturber and sensor locations are marked on the z axis.

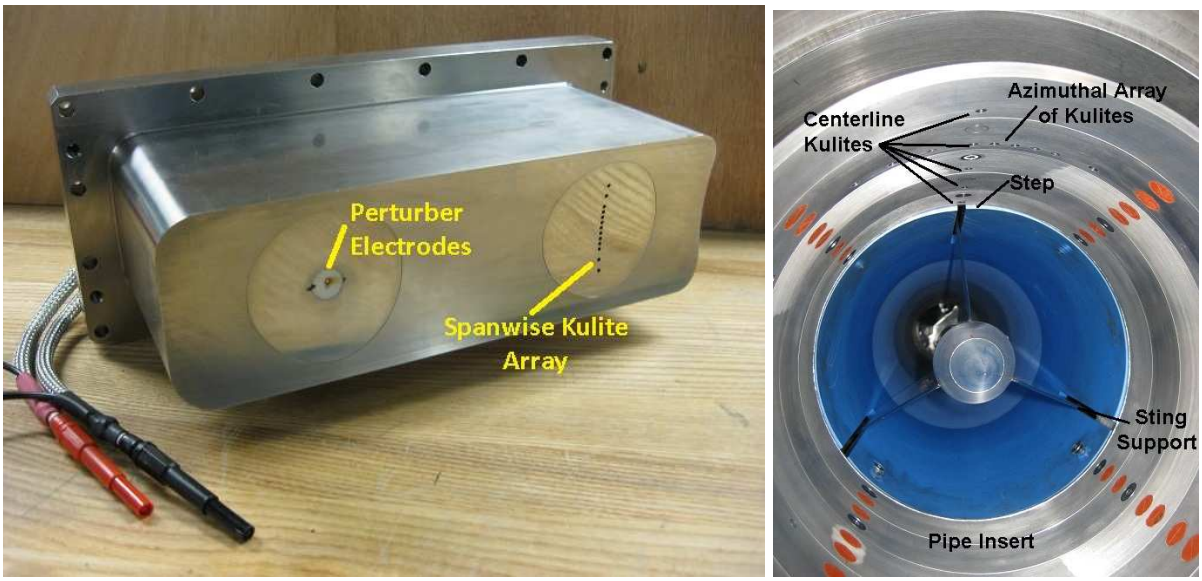

(a) (b)

Figure 3. Pressure instrumentation inserts (a) Upstream insert; (b) Downstream pipe insert.

III. Experimental Results

Measurements of longitudinal merging were made at low, intermediate, and high Re near 6.40, 8.40, and $10.8 \times 10^6/m$, respectively. These measurements were made at freestream conditions similar to the measurements in Casper et al.[13–16] Because the perturbations were repeated at 200 Hz, multiple disturbances can be averaged to reduce electrical noise. The averaging trigger was the 200-Hz square-wave input signal to the perturber. Ensemble-averaged pressure traces of a 4.8-ms time period after the spark were computed for 50 disturbances. These traces were chosen from a 0.5-s interval of a run, after the perturber had been running for a few tenths of a second. More repeatable results were obtained after the perturber had warmed up. Also, even though Re drops within this 0.5-s interval, the change was smaller than 4% and no noticeable effects are seen in the results. Any disturbances that were contaminated by naturally-occurring turbulent spots were not used in the averages. These natural disturbances occurred infrequently and were identified using an RMS threshold criteria on the laminar boundary-layer data measured by a single sensor between glow-induced disturbances. An upstream nozzle-wall sensor was used for this criteria since glow-induced disturbances are still small within the nozzle and the majority of the measured pressure traces contain undisturbed laminar boundary layer data.

Spanwise measurements are used to create contour plots of the disturbances. The results are shown as a function of y, where y is the spanwise coordinate along the circumference of the nozzle wall. Time traces of the pressure fluctuations at each y location were converted to an approximate streamwise coordinate using an average disturbance convection velocity ($\tilde{z} = -tU_c$). This convection velocity varied with Re between 0.79 and 0.84 U_∞.[16] The zero time origin was picked in order to center the disturbances in each plot. This origin will vary for measurements made at different axial locations or different times during a run.

This conversion invokes Taylor's hypothesis which assumes the flow is 'frozen' as it convects over the sensor.[29] This hypothesis is frequently used in the analysis of turbulent flow and has been shown to be a reasonable assumption for many cases, even for low-frequency fluctuations.[30] In the present case, the disturbances will grow in length as they convect over the sensors, but this conversion allows a reasonable approximation of the spatial footprint of the disturbances to be studied. When the time traces are converted to distance, a smaller time corresponds to a greater $\tilde{z}$ location. As a result, the front or leading edge of the disturbances corresponds to smaller t and larger $\tilde{z}$ while the rear or trailing edge of the spot corresponds to larger t and smaller $\tilde{z}$. References to 'upstream' and 'downstream' still correspond to the freestream flow direction in the tunnel.

The zero pressure contour lines were removed from the resulting plots and replaced by minimum contour lines at $\pm$ 0.05 p'/p_∞ in order to compare the spanwise extent of the disturbances between varying Re. Other contour lines are displayed at intervals of 0.2 p'/p_∞. The overall scale of the plots is changed for each case to better show the details of the disturbance structure.

Fig. 4 shows contour plots of ensemble-averaged disturbances at z = 2.781 m for an intermediate Re of 8.40×10^6/m. At a large perturbation spacing of 1.0 ms, the two disturbances look independent. Both disturbances show the characteristic arrowhead shape of a turbulent spot and occupy approximately the same spatial extent. However, as disturbances are repeated at faster rates, the trailing (upstream) disturbance begins to visibly weaken, which is evident in the reduced pressure-fluctuation amplitude and smaller spatial extent of the disturbance. It eventually blends into the low pressure region behind the leading disturbance. The trailing disturbance is only distinguishable, when compared to an isolated disturbance, as weak oscillations in the calmed region behind the original spot. In all cases, the turbulent region of the leading disturbance is unaffected by the presence of the trailing disturbance.

When interpreting these results, the performance of the perturbation itself must be considered, for fast repetition rates. There is a lot of uncertainty in how the pulsed glow perturbation couples with the flow and creates boundary-layer disturbances. There is also uncertainty in how the perturber operates when pulses are generated in rapid succession. Fig. 5(a) shows ensemble-averaged power measurements of the perturber when operated at varying Δt_p. The first perturbation in each pair appears repeatable; however, the trailing perturbations for Δt_p = 0.25–0.50 ms indicate reduced amplitudes. For Δt_p = 1.0 ms, the trailing perturbation appears similar in amplitude to the initial disturbance. However, these ensemble-averaged traces emphasize the low-frequency, high-amplitude content of the perturbation. The important component of this perturbation is the high frequency content between 35–60 kHz that will couple with the boundary layer and lead to the growth of second-mode instability waves on the nozzle wall. In order to show how this high-frequency content changes at fast repetition rates, a power-spectral density of the perturbation power was computed for both the first and second pulses at varying Δt_p (Fig. 5(b)). There are differences

between the first and second perturbations. The first perturbations have higher-amplitude frequency content below 10 kHz. This low-frequency content is visually evident in Fig. 5(a) in the higher amplitude of the overall low-frequency pulse. The first perturbations also have significantly larger high-frequency content. The second perturbations all have similar high-frequency content throughout the spectra, though it is lower than the first perturbations.

In order to study the effect of these nonuniform perturbations, the initial formation of boundary-layer disturbances was measured just downstream of the perturber at z = 2.055 m (Fig. 6(a)). Small low-frequency disturbances have just formed and have not yet begun to interact. The first disturbances created by the perturber are repeatable for all Δt_p. However, there are differences in the trailing disturbances. For Δt_p = 0.25–0.50 ms, the trailing disturbances have a similar shape to the leading disturbances, but they are all smaller in amplitude. Only the trailing disturbance for Δt_p = 1.0 ms has as large an amplitude as the initial disturbance. These measurements reflect the spectra shown in Fig. 5(b). The leading perturbations, as well as the trailing perturbation for Δt_p = 1.0 ms, have a higher level of low-frequency content in the input perturbation. This leads to a higher-amplitude, low-frequency disturbance at z = 2.055 m. Unfortunately, second-mode waves have not grown enough to be observed in the time traces at this location. Only the low-frequency component of the disturbance is seen. Downstream, this low-frequency portion grows slightly, but then much larger second-mode instabilities develop on top of this disturbance and evolve into large wave packets along the nozzle wall. This growth is described in detail in Refs. 13–16.

Centerline measurements further downstream at z = 2.730, 2.781 and 2.831 m are shown in Figs. 6(b) through 6(d). Second-mode instability wave packets have developed by z = 2.730 m. The leading instability wave packet is larger than the trailing wave packets for all Δt_p. This larger leading wave packet may be the result of a higher-amplitude input perturbation at the second-mode wave frequencies (Fig. 5(b)). However, there is a clear trend in the strength of the trailing disturbances, especially at z = 2.730 m. As the spacing between the two disturbances is decreased, the amplitude of the second disturbance also decreases. However, no such trend is seen in the high-frequency region of the perturber power spectra in Fig. 5(b). This trend suggests that a longitudinal merging effect may be responsible, rather than a decay in the perturbation energy. This same trend is also seen in individual samples (Fig. 7), so it is not an effect of any suppression by ensemble averaging. While this result points to suppression of the trailing disturbances by longitudinal merging, there is still significant uncertainty because of the difficulties in isolating the effect of the nonuniform input perturbation.

These plots also show how the trailing disturbance eventually merges with the leading disturbance. The convection velocities of the individual merging disturbances appear the same as isolated disturbances. Because the leading edge of the second disturbance travels faster than the trailing edge of the first disturbance, the second disturbance eventually overtakes and merges with the leading disturbance. During this merging, the internal pressure of the trailing spot will be different than what is suggested by an isolated spot.

These preliminary results are consistent with DNS results of Krishnan et al. and earlier subsonic experiments.[19–23] The calmed region behind the first spot has a more full velocity profile and a lower pressure. As a result, the second disturbance sees a favorable pressure gradient and more stable boundary layer when it encounters the calmed region. This causes the second disturbance to grow more slowly.

At the highest *Re* of 10.8×10^6/m, the growth of the trailing turbulent spot is again reduced at fast repetition rates and therefore closer spot proximity (Fig. 8). For Δt_p = 1.0 ms, the two turbulent spots appear similar. They are sufficiently far apart that they have not begun to interact. For Δt_p = 0.50 ms, a smaller trailing disturbance is seen. This disturbance still has an arrowhead shape of a turbulent spot, but the magnitude of the internal pressure fluctuations are much smaller. This smaller trailing disturbance may be, at least in part, the result of a smaller input perturbation at the second-mode wave frequencies as shown in Fig. 5(b). However, between Δt_p = 0.5 and 0.25 ms, a further reduction of the trailing disturbance is clearly seen as the second disturbance enters the calmed region of the first. The positive pressure fluctuations seen for Δt_p = 0.50 ms are no longer seen at smaller Δt_p. Also, the lateral growth of the second disturbance is reduced between Δt_p = 0.50 and 0.25 ms. Some fluctuations are seen outside the spanwise edges of the calmed region for Δt_p = 0.50 ms, but those fluctuations are no longer seen for Δt_p = 0.25 ms.

Centerline measurements again show that a constant, but smaller amplitude, trailing disturbance is measured at z = 2.055 m for Δt_p = 0.25–0.5 ms (Fig. 9). This result is again consistent with the power spectra of the input perturbation (Fig. 5(b)) which shows larger frequency content below 10 kHz for the first perturbations as well as the second perturbation at Δt_p = 1.0 ms. Downstream between z = 2.730–2.831 m, a clear trend of suppression of the trailing disturbance is seen as Δt_p is reduced, even though the

high-frequency content of the second perturbations appears constant for all Δt_p. This result again points to a longitudinal merging effect. Without longitudinal merging, the second perturbations should all have the same amplitude since the input perturbation has similar content at the second-mode wave frequencies.

Similar results were obtained at a low Re of $6.40 \times 10^6/m$ (Figs. 10 and 11). At this condition, disturbances remain wave packets over the measurement area. With $\Delta t_p = 1.0$ ms, the two disturbances appear similar. They both show a characteristic wave packet signature with alternating positive and negative pressures. The wave packets are still small, so the spanwise extent of the disturbances is limited. When the disturbances are created much closer together with $\Delta t_p = 0.5$ ms, the two disturbances are different. The second disturbance is smaller than the first, and the pressure fluctuations are greatly reduced. This smaller trailing disturbance is probably once again a combined effect of a smaller second glow perturbation and a longitudinal merging effect. As the disturbances are created closer together with $\Delta t_p = 0.33$ and 0.25 ms, the growth of the second wave packet is much smaller and the two disturbances have effectively combined into one. Only a few extra weak oscillations can be seen compared to an isolated disturbance. In this case, it is interesting to note that there is a small amount of increased lateral spreading of the wave packet during this interaction. This is most evident for $\Delta t_p = 0.33$ and 0.25 ms. This increased lateral spreading is different than seen for $Re = 10.8 \times 10^6/m$ where there was a slightly smaller lateral extent of the trailing disturbance.

IV. Concluding Remarks

A preliminary study of the longitudinal merging of controlled wave packets and turbulent spots was conducted on the nozzle wall of the BAM6QT. These new measurements complement the studies of isolated disturbances reported in Casper et al.[13–16] Two pulsed glow perturbations were generated in quick succession in order to create two closely spaced disturbances. These disturbances developed into wave packets at lower Re and turbulent spots at higher Re. By changing the temporal spacing between the two perturbations, longitudinal merging of the disturbances could be simulated. These experiments look at how merging can affect the internal pressure structure and spatial growth of the turbulent spots. These are important parameters for a turbulent-spot model of the transitional fluctuations. The suppression of the trailing disturbance is not included in the classical intermittency model of transition.

These preliminary results suggest that the growth of the trailing (upstream) disturbance may be suppressed by the leading disturbance. There are smaller pressure fluctuations within the core of the trailing spot, and the lateral extent of the trailing disturbances is somewhat altered. However, the core of the leading disturbance appears unaffected by the presence of the trailing disturbance. The calmed region downstream of the leading spot acts to suppress the growth of the trailing disturbance. Only small fluctuations indicating the presence of the trailing disturbance are evident in the calmed region once this merging has occurred. These results appear consistent with DNS computations on a flat plate at Mach 2 as well as with several low-speed experiments.[19–23]

While these measurements point to a longitudinal merging effect, results must be considered inconclusive because of the variation of the perturber behavior at rapid repetition rates and the uncertainty in how the perturbations couple with the flow. It is difficult to separate this nonuniform perturber behavior from the possible longitudinal merging effect. However, the present results point the way towards some interesting and necessary understanding of the spot merging process that will be important for transition model development. In the future, a more repeatable perturber will be developed that can reliably operate at fast repetition rates. These measurements will be conducted again with this improved perturber in order to unambiguously show this longitudinal merging effect.

Acknowledgments

This work could not have been completed without the help of John Phillips, the Purdue AAE department electronics technician, who designed and built the perturber used for these measurements. Peter Gilbert provided the CAD model used to generate Fig. 2. Funding was provided in part by the National Science Foundation Graduate Research Fellowship Program, Sandia National Laboratories, and AFOSR.

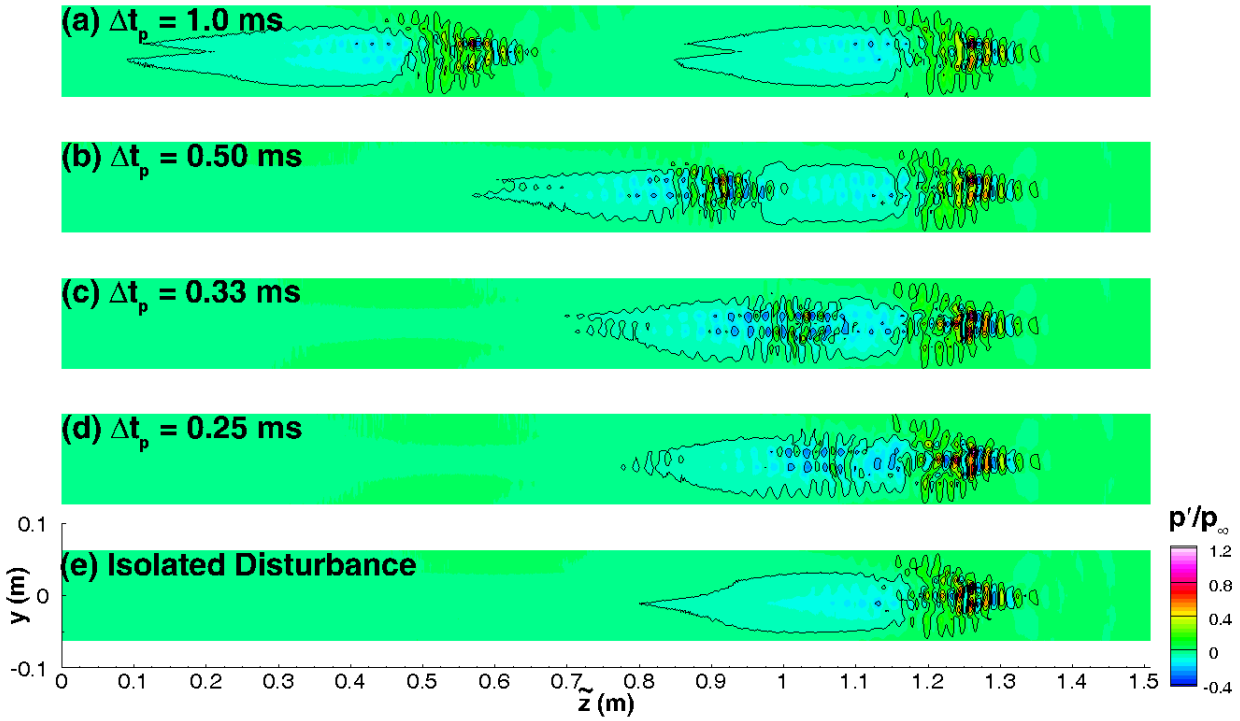

Figure 4. Ensemble-averaged disturbances generated at varying intervals Δt_p near $Re = 8.40 \times 10^6/\text{m}$, z = 2.781 m.

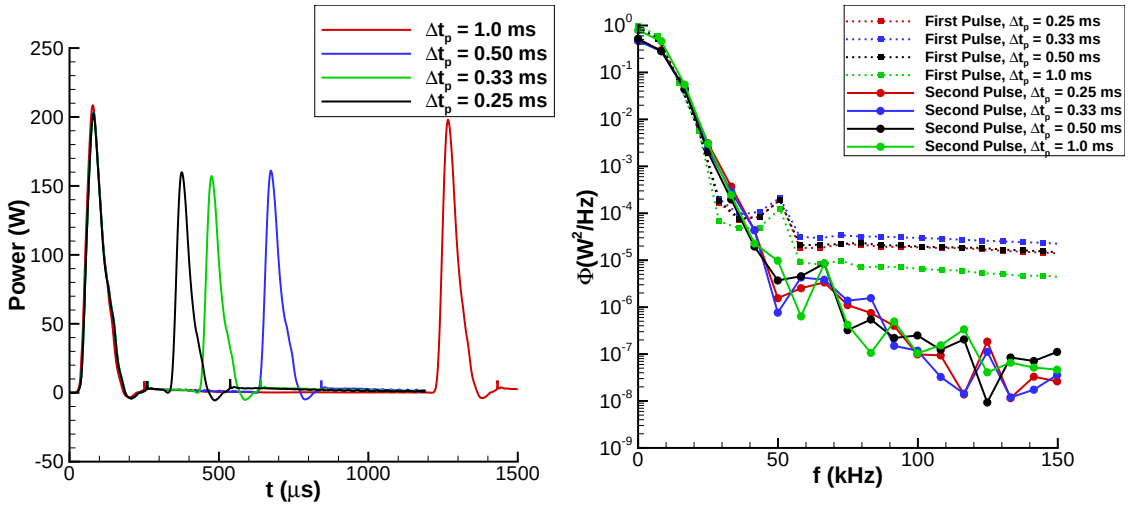

(a) (b)

Figure 5. Power measurements of repeated perturbations near $Re = 6.40 \times 10^6/m$ (a) Ensemble-averaged power traces; (b) Power spectral density.

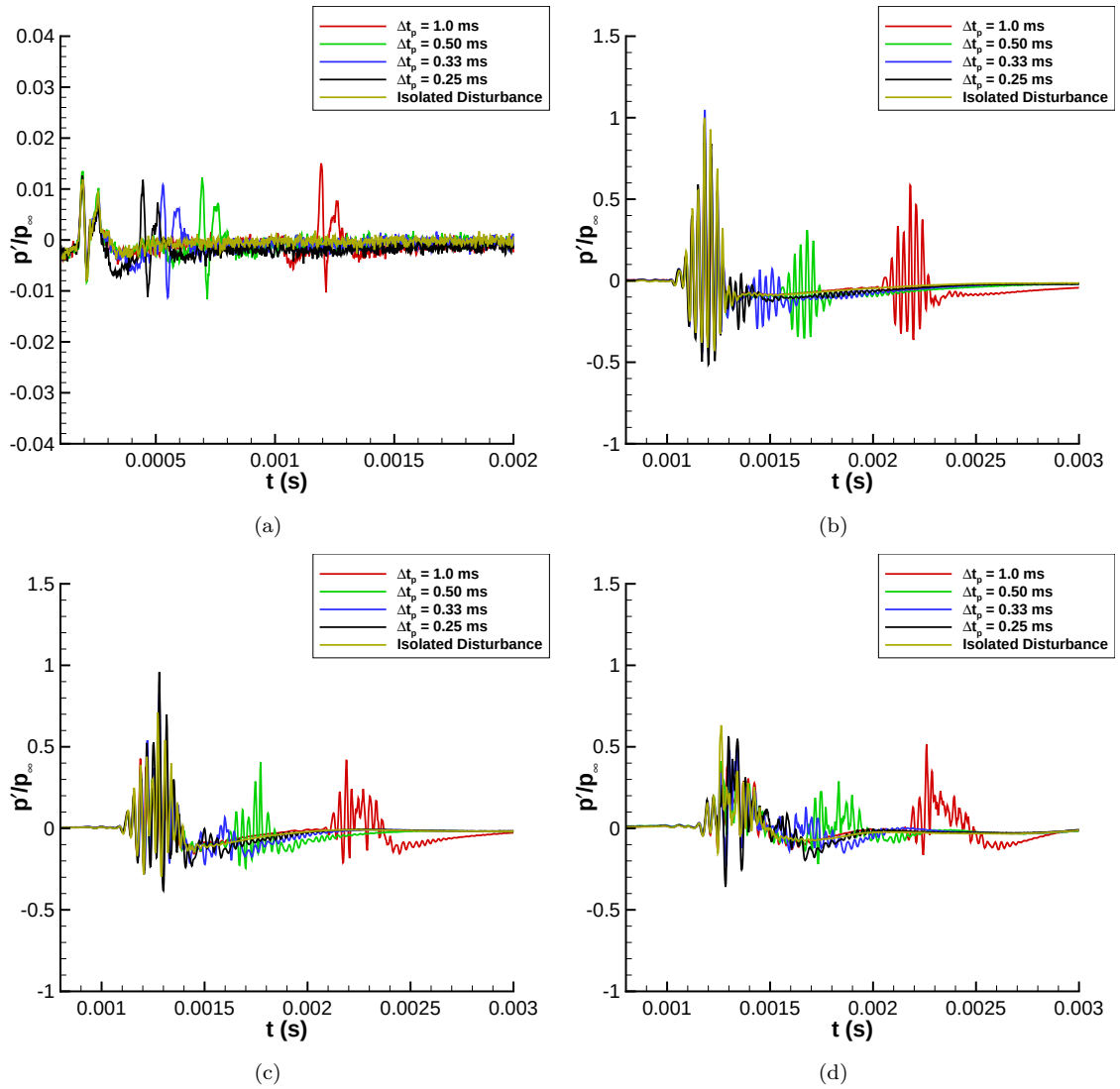

Figure 6. Ensemble-averaged centerline measurements of merging disturbances near $Re = 8.40 \times 10^6/m$ **(a) z = 2.055 m; (b) z = 2.730 m; (c) z = 2.781 m; (d) z = 2.831 m.**

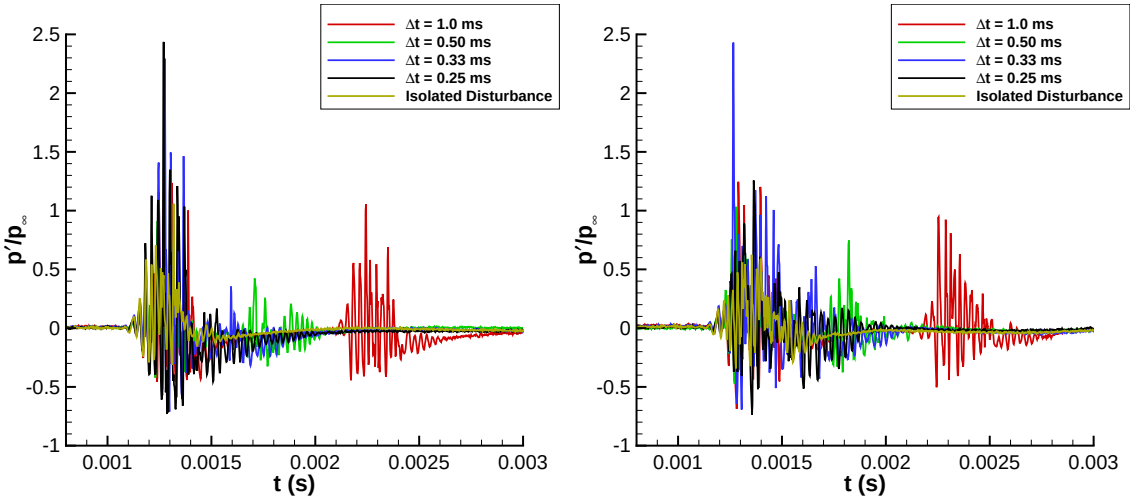

Figure 7. Centerline measurements of merging disturbances near $Re = 8.40 \times 10^6/m$, individual samples (a) z = 2.781 m; (b) z = 2.831 m.

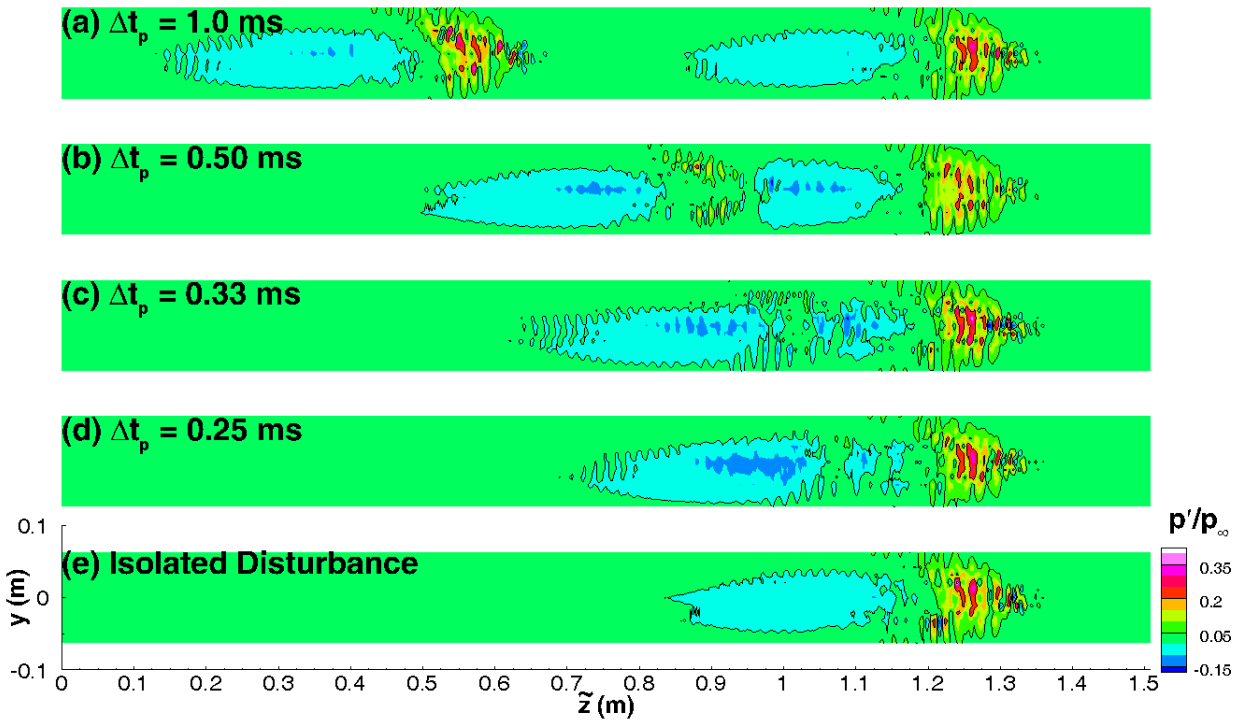

Figure 8. Ensemble-averaged disturbances generated at varying intervals Δt_p near $Re = 10.8 \times 10^6$/m, z = 2.781 m.

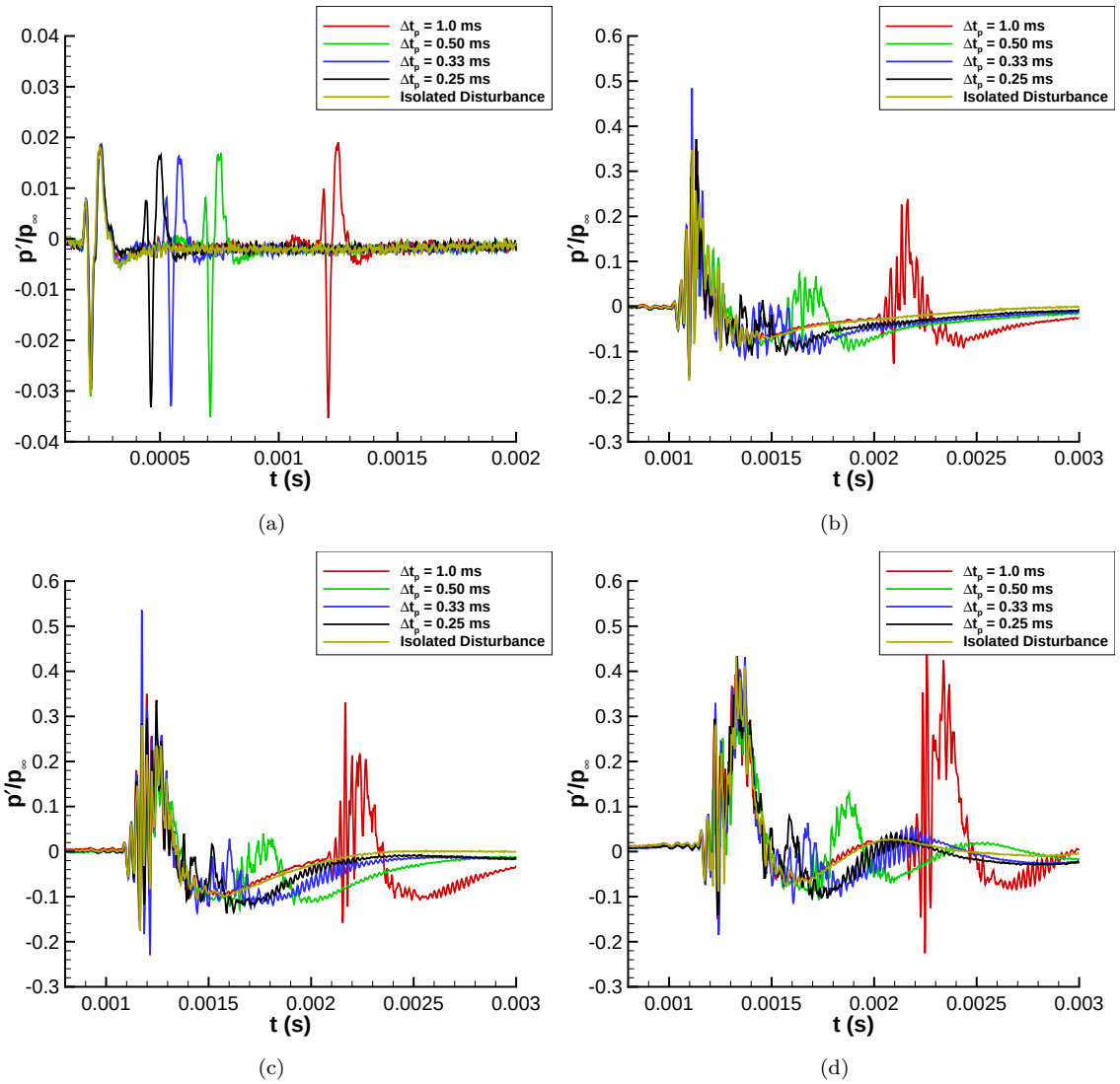

Figure 9. Ensemble-averaged centerline measurements of merging disturbances near $Re = 10.8 \times 10^6/m$ **(a) z = 2.055 m; (b) z = 2.730 m; (c) z = 2.781 m; (d) z = 2.831 m.**

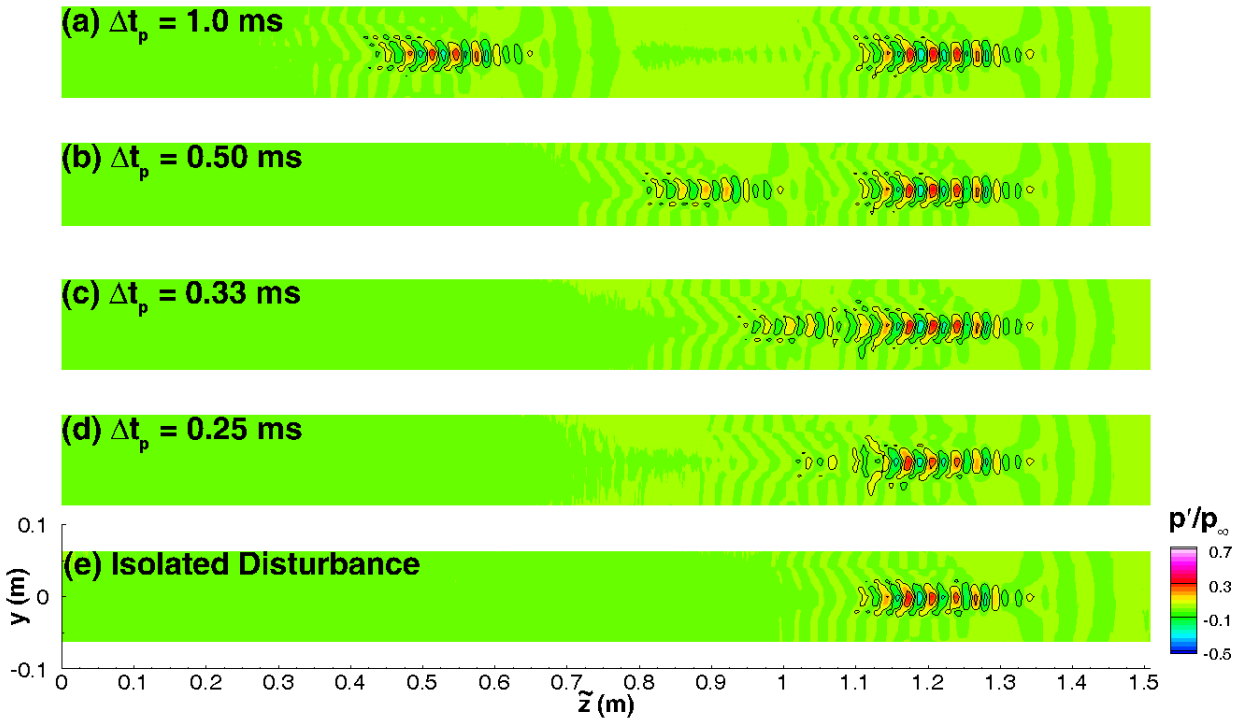

Figure 10. Ensemble-averaged disturbances generated at varying intervals Δt_p near $Re = 6.40 \times 10^6$/m, z = 2.781 m.

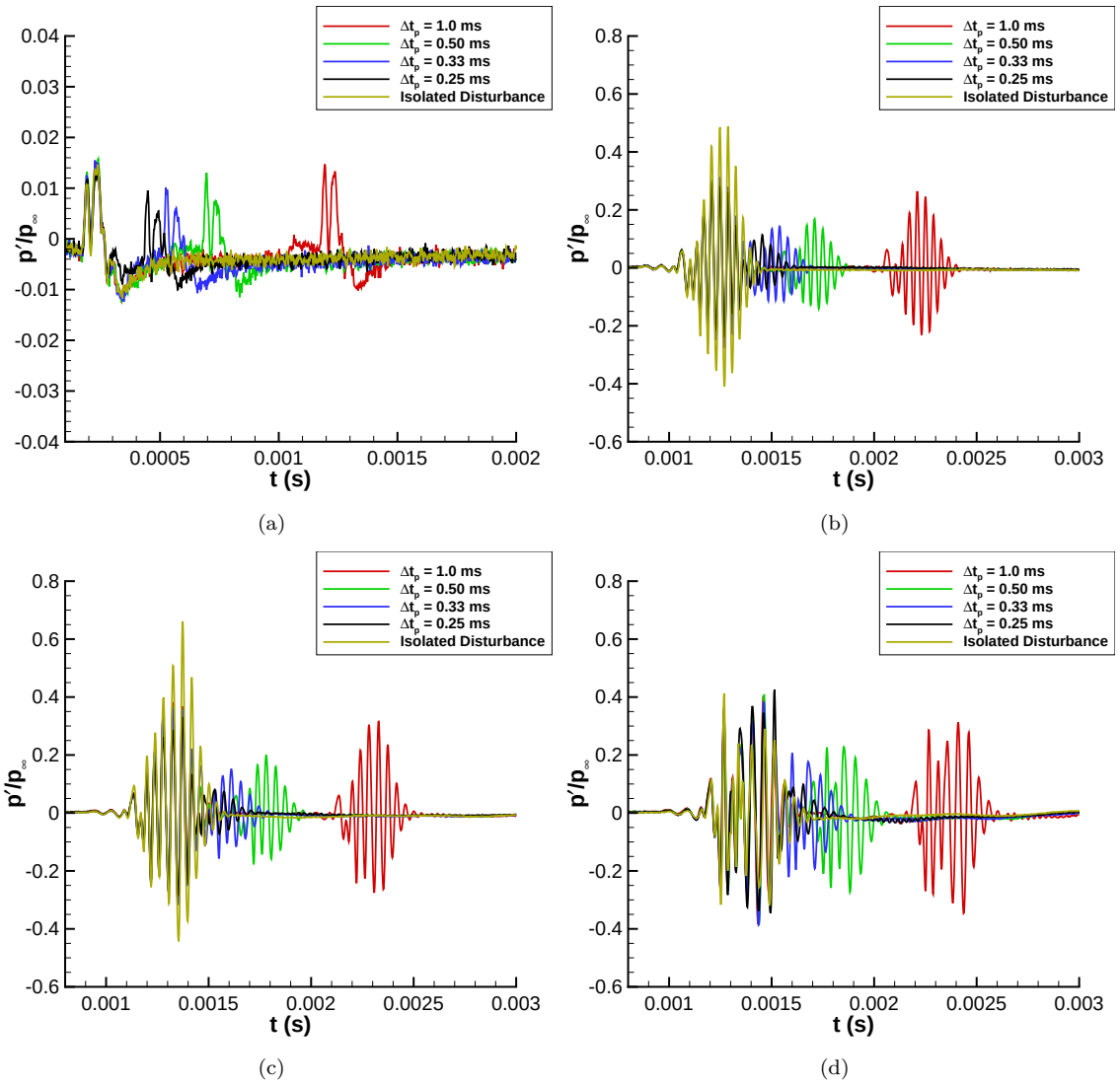

Figure 11. Ensemble-averaged centerline measurements of merging disturbances near $Re = 6.40 \times 10^6/m$ **(a) z = 2.055 m; (b) z = 2.730 m; (c) z = 2.781 m; (d) z = 2.831 m.**

References

[1]Laganelli, A. L., Martellucci, A., and Shaw, L. L., "Wall Pressure Fluctuations in Attached Boundary-Layer Flow," *AIAA Journal*, Vol. 21, No. 4, 1983, pp. 495–502.

[2]Pate, S. R. and Brown, M. D., "Acoustic Measurements in Supersonic Transitional Boundary Layers," AEDC-TR-69-182, October 1969.

[3]Johnson, R. I., Macourek, M. N., and Saunders, H., "Boundary Layer Acoustic Measurements in Transitional and Turbulent Flow at $M_\infty = 4.0$," AIAA Paper 69-344, April 1969.

[4]Cassanto, J. M. and Rogers, D. A., "An Experiment to Determine Nose Tip Transition with Fluctuating Pressure Measurements," *AIAA Journal*, Vol. 13, No. 10, October 1975, pp. 1257–1258.

[5]Martellucci, A., Chaump, L., Rogers, D., and Smith, D., "Experimental Determination of the Aeroacoustic Environment about a Slender Cone," *AIAA Journal*, Vol. 11, No. 5, 1973, pp. 635–642.

[6]Pate, S. R., "Dominance of Radiated Aerodynamic Noise on Boundary-Layer Transition in Supersonic/Hypersonic Wind Tunnels," AEDC-TR-77-107, March 1978.

[7]Narasimha, R., "The Laminar-Turbulent Transition Zone in the Boundary Layer," *Progress in Aerospace Sciences*, Vol. 22, January 1985, pp. 29–80.

[8]Park, S. and Lauchle, G., "Wall Pressure Fluctuation Spectra Due to Boundary-Layer Transition," *Journal of Sound and Vibration*, Vol. 319, 2009, pp. 1067–1082.

[9]Krishnan, L. and Sandham, N. D., "Effect of Mach Number on the Structure of Turbulent Spots," *Journal of Fluid Mechanics*, Vol. 566, 2006, pp. 225–234.

[10]Joksch, A. and Kleiser, L., "Growth of Turbulent Spots in High-Speed Boundary Layers on a Flat Plate," *International Journal of Heat and Fluid Flow*, Vol. 29, 2008, pp. 1543–1557.

[11]Sivasubramanian, J. and Fasel, H. F., "Direct Numerical Simulation of a Turbulent Spot in a Cone Boundary-Layer at Mach 6," AIAA Paper 2010-4599, June 2010.

[12]Sivasubramanian, J. and Fasel, H. F., "Transition Initiated by a Localized Disturbance in a Hypersonic Flat-Plate Boundary Layer," AIAA Paper 2011-374, January 2011.

[13]Casper, K., Beresh, S., and Schneider, S., "Pressure Fluctuations Beneath Turbulent Spots and Instability Wave Packets in a Hypersonic Boundary Layer," AIAA Paper 2011-372, January 2011.

[14]Casper, K., Beresh, S., and Schneider, S., "Spanwise Growth of the Turbulent Spot Pressure-Fluctuation Field in a Hypersonic Boundary Layer," AIAA Paper 2011-3873, June 2011.

[15]Casper, K., Beresh, S., and Schneider, S., "Characterization of Controlled Perturbations in a Hypersonic Boundary Layer," AIAA Paper 2012-281, January 2012.

[16]Casper, K., *Pressure Fluctuations Beneath Instability Wave Packets and Turbulent Spots in a Hypersonic Boundary Layer*, Ph.D. Thesis, Purdue University, School of Aeronautics & Astronautics, to appear August 2012.

[17]Emmons, H. W., "The Laminar-Turbulent Transition in a Boundary Layer – Part I," *Journal of the Aeronautical Sciences*, Vol. 18, No. 7, 1951, pp. 490–498.

[18]Elder, J. W., "An Experimental Investigation of Turbulent Spots and Breakdown to Turbulence," *Journal of Fluid Mechanics*, Vol. 9, No. 2, 1960, pp. 235–246.

[19]Zilberman, M., Wygnanski, I., and Kaplan, R. E., "Transitional Boundary Layer Spot in a Fully Turbulent Environment," *Physics of Fluids*, Vol. 20, 1977, pp. S258–S271.

[20]Savas, O., *Some Measurements in Synthetic Turbulent Boundary Layers*, Ph.D. Thesis, California Institute of Technology, 1979.

[21]Gutmark, E. and Blackwelder, R. F., "On the Structure of a Turbulent Spot in a Heated Boundary Layer," *Experiments in Fluids*, Vol. 5, 1987, pp. 217–229.

[22]Makita, H. and Nishizawa, A., "Characteristics of Internal Vortical Structures in a Merged Turbulent Spot," *Journal of Turbulence*, Vol. 2, No. 12, 2001, pp. 1–14.

[23]Krishnan, L. and Sandham, N. D., "On the Merging of Turbulent Spots in a Supersonic Boundary Layer Flow," *International Journal of Heat and Fluid Flow*, Vol. 27, March 2006, pp. 542–550.

[24]Keyes, F. G., "A Summary of Viscosity and Heat-Conduction Data for $He, A, H_2, O_2, N_2, CO, CO_2, H_2O$, and Air," *Transactions of the ASME*, Vol. 73, 1951, pp. 589–596.

[25]Steen, L. E., *Characterization and Development of Nozzles for a Hypersonic Quiet Wind Tunnel*, Master's Thesis, Purdue University, School of Aeronautics & Astronautics, December 2010.

[26]Schneider, S. P., "The Development of Hypersonic Quiet Tunnels," *Journal of Spacecraft and Rockets*, Vol. 45, No. 4, 2008, pp. 641–664.

[27]Beresh, S. J., Henfling, J. F., Spillers, R. W., and Pruett, B. O. M., "Fluctuating Wall Pressures Measured Beneath a Supersonic Turbulent Boundary Layer," *Physics of Fluids*, Vol. 23, 075110, 2011.

[28]Rotea, M. A., Randall, L. A., Song, G., and Schneider, S. P., "Model Identification of a Kulite Pressure Transducer," AIAA Paper 96-2278, June 1996.

[29]Taylor, G. I., "The Spectrum of Turbulence," *Proceedings of the Royal Society of London*, Vol. 164, 1938, pp. 476–490.

[30]Dennis, D. J. C. and Nickels, T. B., "On the Limitations of Taylors Hypothesis in Constructing Long Structures in a Turbulent Boundary Layer," *Journal of Fluid Mechanics*, Vol. 614, 2008, pp. 197–206.